Towards Replacing Late Gadolinium Enhancement With Artificial Intelligence Virtual Native Enhancement For Gadolinium-free Cardiovascular Magnetic Resonance Tissue Characterization in Hypertrophic Cardiomyopathy

Qiang Zhang, PhD[1,2], **Matthew K. Burrage, MBBS FRACP**[1,2], **Elena Lukaschuk, MSc**[1,2], **Mayooran Shanmuganathan, MBBS MRCP**[1,2], **Iulia A. Popescu, DPhil**[1,2], **Chrysovalantou Nikolaidou, MD**[1,2], **Rebecca Mills, BSc**[1,2], **Konrad Werys, PhD**[1,2], **Evan Hann, DPhil**[1,2], **Ahmet Barutcu, MD**[1], **Suleyman D. Polat, MD**[1], **HCMR investigators**[†], **Michael Salerno, MD, PhD**[3], **Michael Jerosch-Herold, PhD**[4], **Raymond Y. Kwong, MD, MPH**[4], **Hugh C. Watkins, MD, PhD**[1,2], **Christopher M. Kramer, MD**[3], **Stefan Neubauer, MD**[1,2], **Vanessa M. Ferreira, MD DPhil**[1,2,*], **Stefan K. Piechnik, DSc, PhD**[1,2,*]

[1.]Oxford Centre for Clinical Magnetic Resonance Research, Oxford BRC NIHR, Division of Cardiovascular Medicine, Radcliffe Department of Medicine, University of Oxford, Oxford, United Kingdom

[2.]Radcliffe Department of Medicine, University of Oxford, Oxford, United Kingdom

[3.]Department of Medicine, University of Virginia Health System, Charlottesville, Virginia, USA

[4.]Cardiovascular Division, Department of Medicine, Brigham and Women's Hospital, Harvard Medical School, Boston, Massachusetts, USA

Abstract

Background: Late gadolinium enhancement (LGE) cardiovascular magnetic resonance (CMR) imaging is the gold standard for non-invasive myocardial tissue characterization, but requires intravenous contrast agent administration. It is highly desired to develop a contrast-agent-free technology to replace LGE for faster and cheaper CMR scans.

Methods: A CMR Virtual Native Enhancement (VNE) imaging technology was developed using artificial intelligence. The deep learning model for generating VNE uses multiple streams of convolutional neural networks to exploit and enhance the existing signals in native T1-maps (pixel-wise maps of tissue T1 relaxation times) and cine imaging of cardiac structure and function, presenting them as LGE-equivalent images. The VNE generator was trained using generative

Correspondence: Qiang Zhang, Oxford Centre for Clinical Magnetic Resonance Research (OCMR), Level 0, John Radcliffe Hospital, Headington, Oxford, United Kingdom, OX3 9DU. qiang.zhang@cardiov.ox.ac.uk, Tel: +44 (0) 7442336388.
*Joint senior authors
†List of the HCMR investigators provided in the Supplement

Supplemental Materials

Supplemental Figures I – IX

Supplemental Table I

Expanded Methods: Deep Learning Technical Details.

Supplemental Content: HCMR investigators.

References: [49–52]

adversarial networks. This technology was first developed on CMR datasets from the multi-center Hypertrophic Cardiomyopathy Registry (HCMR), using HCM as an exemplar. The datasets were randomized into two independent groups for deep learning training and testing. The test data of VNE and LGE were scored and contoured by experienced human operators to assess image quality, visuospatial agreement and myocardial lesion burden quantification. Image quality was compared using nonparametric Wilcoxon test. Intra- and inter-observer agreement was analyzed using intraclass correlation coefficients (ICC). Lesion quantification by VNE and LGE were compared using linear regression and ICC.

Results: 1348 HCM patients provided 4093 triplets of matched T1-maps, cines, and LGE datasets. After randomization and data quality control, 2695 datasets were used for VNE method development, and 345 for independent testing. VNE had significantly better image quality than LGE, as assessed by 4 operators (n=345 datasets, p<0.001, Wilcoxon test). VNE revealed characteristic HCM lesions in high visuospatial agreement with LGE. In 121 patients (n=326 datasets), VNE correlated with LGE in detecting and quantifying both hyper-intensity myocardial lesions (r=0.77–0.79, ICC=0.77–0.87; p<0.001) and intermediate-intensity lesions (r=0.70–0.76, ICC=0.82–0.85; p<0.001). The native CMR images (cine plus T1-map) required for VNE can be acquired within 15 minutes. Producing a VNE image takes less than one second.

Conclusions: VNE is a new CMR technology that resembles conventional LGE, without the need for contrast administration. VNE achieved high agreement with LGE in the distribution and quantification of lesions, with significantly better image quality.

Keywords

Introduction

Late gadolinium enhancement (LGE) cardiovascular magnetic resonance (CMR) imaging is well-validated for detecting focal myocardial lesions and fibrosis in a variety of cardiovascular diseases [1–5]. The presence and extent of LGE is independently associated with adverse outcomes, including in hypertrophic cardiomyopathy (HCM) [6–11]. However, LGE requires intravenous injection of a gadolinium-based contrast agent (GBCA), which is cautioned in patients with severe kidney failure and contraindicated in those with known GBCA allergy [12]. Eliminating the need for GBCA administration could significantly shorten scan times, reduce costs of associated consumables, shorten patient preparation time, and circumvent the need for physician presence.

Native (pre-contrast) CMR modalities are alternative means for tissue characterization without the need for GBCA. Cine imaging consists of a sequence of images at different cardiac phases to assess the cardiac structure and motion. Native T1-mapping estimates the T1 (proton spin-lattice) relaxation time of tissues on a pixel-by-pixel basis. Native T1-mapping exhibits sensitivity to a variety of cardiac diseases [13], including early myocardial changes in HCM [14–16]. Abnormal T1 signals correlate to areas of LGE and on histopathology in models of focal and diffuse fibrosis [17–19]. Native T1-mapping appears

the most promising GBCA-free technique to reveal intrinsic imaging signals associated with myocardial abnormalities seen in LGE. However, the clinical utility of T1-mapping has largely been hindered by a lack of standardized interpretation and post-processing, confounding factors and diagnostic specificity [13, 20].

We hypothesized that native T1-maps may be transformed into visually diagnostic images similar to LGE images. In this work, using novel artificial intelligence (AI) approaches, a Virtual Native Enhancement (VNE) imaging technology was developed, which exploits and enhances existing contrast and signals within the native T1-maps and cine frames, and displays them in a standardized presentation. The VNE imaging was then validated by comparing against matching LGE for image quality, visuospatial agreement, and myocardial lesion quantification. The approach was developed first in HCM, partly because it is an important indication for LGE assessment in its own right, but also because its features of regional heterogeneity and diverse tissue remodeling processes make it a good test case for a wide range of cardiac pathology.

Methods

The anonymized test data that support the findings of this study are available from the corresponding author upon reasonable request and subject to multicenter Hypertrophic Cardiomyopathy Registry (HCMR) committee approval.

Deep learning method for Virtual Native Enhancement

The proposed VNE technology uses two native components: native T1-mapping (including the native inversion recovery-weighted (IRW) images) and pre-contrast cine frames of a cardiac cycle. IRW images and T1-maps provide image contrast and signal changes in myocardial tissue properties. Cine frames provide additional wall motion information and more defined myocardial borders. These images were input into a deep learning generator to derive a VNE image (Figure 1B).

Neural Network Design.—The VNE generator has three parallel convolutional neural network streams to process cine frames, IRW images and T1-maps, respectively. Each stream has an encoder-decoder U-Net [21] architecture (Figure 1B). The encoder successively computes image features from fine to coarse, providing a multi-scale feature representation. The decoder combines the multi-scale features to produce final feature maps. The three streams of feature maps by U-Nets are concatenated and input into a further neural network block to fuse the information from multi-modalities and produce a final VNE image.

Neural Network Training.—The neural networks were trained using a modified conditional Generative Adversarial Network approach [22], which optimizes the VNE generator together with a "discriminator". This VNE application focused on the enhancement of native CMR signals and presenting them as VNE that resembles LGE images. This was achieved by defining the objective of the generator to produce VNE images that match LGE in perceptual similarity – a higher deep learning feature comparison using a pre-trained neural network (VGG-net) [23] – and that are indistinguishable from

LGE contrast. The objective of the "discriminator" is to distinguish between VNE and LGE images. The two neural networks were trained in an adversarial manner. This strategy resulted in a trained generator that translates the existing native CMR signals into LGE representation. For reproducibility, full deep learning details are provided in Expanded Methods in the Supplement. Once trained, generating a VNE image takes ~50 milliseconds on GPU, or 130 milliseconds on a modern CPU. The generated VNE images have the same spatial resolution as the T1-maps.

Materials for validation of the concept

CMR datasets from the large HCMR study [11] were used. This study has institutional review committee approval and ethics approval, and all patients have given written consent. The HCMR [11] scanning protocol included pre-contrast short-axis cine imaging (for assessing cardiac motion and structure) and native T1-mapping (quantitative pixel-wise maps of T1 relaxation time), followed by intravenous administration of 0.1–0.2 mmol/kg GBCA and LGE imaging at ~10 minutes post GBCA (Figure 1A). Each scan has typically three short-axis T1-maps, and whole-heart short-axis coverage for cine and LGE. Short-axis native T1-maps (ShMOLLI [24], protocol checked using a phantom approach [25]), cines (before any administration of GBCA) and LGE images [26] were collected. LGE images were acquired using a conventional and widely-available 2D breath-hold and segmented phase-sensitive inversion-recovery (PSIR) method [11]. The LGE PSIR images were used for developing the deep learning models because of its consistent image appearance due to less sensitivity to the inversion time (TI) setting. T1-maps, cines and LGE images were matched for slice orientation (slice plane cosine similarity >0.9) and position (slice location difference <4mm) using an automated pipeline written in Python. Additional manual quality control was performed to exclude cases with severe artefacts and slice mismatch due to patient movement (Figure 2). All T1-maps have consistent pixel spacing (distance between pixel centers) of approximately 1mm in the datasets. Cine and LGE images were interpolated to match the pixel spacing, image position and orientation to the T1-maps – therefore, a pixel-to-pixel match (see Figure I in the Supplement).

The CMR datasets were randomized into two independent groups for deep learning method development and testing (Figure 2). The development group was further divided into training (90%) and validation (10%) datasets. Deep learning models were blinded to the test group.

Qualitative and quantitative evaluation of VNE and LGE

Three clinical assessors trained in CMR and one CMR radiographer scored the image quality of VNE and LGE guided by a 5-point categorical scale: "uninterpretable", "poor quality", "acceptable quality", "good quality" and "excellent quality" that is intuitive for human operators (Figure II in the Supplement, interface by IAP). Behind the interface, the score was recorded on a numerical scale between 0–100 for statistical analyses (see an example in Figure II F). The quality aspects considered included motion artefacts, noise, image contrast, and clarity of tissue borders. The images were randomly shuffled and the operators were blinded to whether the image was VNE or LGE.

Semi-automated myocardial lesion quantification by VNE and LGE was performed as follows: Epicardial and endocardial LV contours were initialized automatically [27] and adjusted manually on all images by an experienced operator (EL, 10 years of experience in CMR image analysis) using MC-ROI (developed by SKP in Interactive Data Language v6.1). A remote reference region of interest (ROI) without LGE was added and lesion burden was calculated using adaptations of the Full Width at Half Maximum (FWHM) method [28]. Specifically, average signal intensities of remote myocardium ROI set the minimum values. Average signal intensities of the LV blood pool center ROIs (avoiding papillary muscles) set the maximum values, for consistency among cases with hyper-intensity, intermediate-intensity signals or no lesions. FWHM thresholding at 50th percentile, despite superior reproducibility, has been reported to underestimate lesion burden in HCM [29]. Therefore, progressive thresholds at 25th and 12.5th percentiles were also used, referred to as full width at quarter maximum (FWQM) and eighth maximum (FWEM), respectively, to capture subtle, intermediate-intensity changes often seen in HCM [30]. Lesion burden was quantified for each patient as the sum of lesion areas divided by the total LV myocardial area in all available short-axis slices.

Statistical analysis

For image quality assessment, the test images were shuffled and scored blindly by all operators, with 20% random images scored repeatedly to calculate intra-observer variability, reported as standard deviation (SD) and intraclass correlation coefficients (ICC). The statistical significance of differences in VNE and LGE quality scores was analyzed using nonparametric Wilcoxon tests. Correlation between lesion burden quantification by VNE and LGE was assessed using linear regression coefficients and ICC. Bland-Altman analysis was performed to analyze any systematic differences between quantification by VNE and LGE. Statistical significance was defined as $p < 0.05$.

Results

Study population

1348 patient CMR datasets met the selection criteria of having matched pre- and post-contrast images (Figure 2), providing 4093 triplets of T1-maps, cines and LGE images from 28 multinational CMR sites. Quality control excluded post-contrast cines, T1-maps with severe artefacts, and mismatched slice locations in the triplets (Figure 2). After this, 2695 triplets of images (from 1075 patients) were available for training of the deep learning methods, and 345 triplets (from 124 patients) for independent testing.

Image quality of VNE and LGE

On head-to-head comparisons, VNE provided significantly better image quality than LGE, as assessed by all 4 independent and blinded operators ($p < 0.001$, Wilcoxon test) (Figure 3A). Intra-observer variability for the four operators was SD = 5.9, 8.3, 6.9, 7.3, and ICC was 0.87, 0.88, 0.89, 0.87. Inter-observer variability was SD = 8.5±0.7 and ICC was 0.83±0.03. For "uninterpretable" (Figure 3A, red clusters, n=19) or "poor" (blue, n=53) LGE cases, VNE improved the quality of all but one image (Figure 3A, dashed line), and was scored as acceptable or above for all but 4 images. Conventional LGE can be affected

by inaccurate TI selection and breathing artefacts due to patient fatigue at the last stage of long scanning sessions (Figure 3B, orange boxed). In contrast, VNE produced more consistent and better image quality (Figure 3B, green boxed). Additionally, VNE images have better-defined shapes and borders (Figure 3B, green boxed), likely inherited from cine images. Cases with "uninterpretable" LGE (5.5%, 19 slices out of 345) were excluded for lesion quantification assessment.

Comparison of myocardial lesion quantification between VNE and LGE

After exclusion of cases with "uninterpretable" LGE (Figure 3A, red clusters, n=19), lesion quantification was performed on 326 short-axis pairs of VNE and LGE images (from 121 patients). VNE lesions were in high visuospatial agreement with LGE, as visually assessed by two CMR experts independently (examples in Figure 4A–F). The lesion regions defined by FWHM, FWQM and FWEM methods (i.e., thresholding at 50th, 25th, 12.5^{th} percentiles) were displayed with three progressive colors to visualize hyper-intensity (red) and intermediate-intensity (yellow to light blue) abnormalities (Figure 4, bottom two rows). VNE revealed characteristic HCM lesions in hypertrophied segments and at the anterior and inferior RV insertion points (Figure 4). Origins of these VNE signals can be seen in corresponding native T1-maps (Figure 4, top row). Despite matched slice position and orientation by image metadata between T1-maps and LGE, some T1-maps and their derived VNE have slightly different image appearance than the corresponding LGE (Figure 4E, yellow arrows). This may be due to slight positional differences due to patient movement between acquisitions of the T1-maps and LGE, despite meticulous checks for such effects (Figure 2, and Figure IV in the Supplement).

On the full 121 test patients, lesion burdens by VNE correlated strongly with LGE in both hyper-intensity lesions (quantified by FWHM), and more subtle intermediate-intensity abnormalities (quantified by FWQM and FWEM). The linear correlation coefficient was R=0.77, 0.75, 0.72, and ICC was 0.77, 0.84, 0.83 for FWHM, FWQM, FWEM, respectively (all p<0.001; Figure 5A–C). Bland-Altman plots showed 5% to 8% average lower lesion burdens by VNE, with asymmetric 95% confidence intervals (upper bound of 11% to 17% and bottom bound −21% to −30%) (Figure 5A–C, bottom panels). These plots also revealed a perceivable skew, which may indicate enhanced signals in VNE for detecting subtle LGE lesions (Figure 5A–C, arrowed), pending future validation. Figure 4G provides an example of subtle lesions in this range, in which VNE showed clearer lesion signals than the corresponding LGE, which also detected the lesions, albeit more subtly.

To achieve comparable lesion quantification between VNE and LGE, adjusted threshold values (e.g., 35th, 20th, 10th percentiles) can be used for VNE, to match with LGE using 50th, 25th, 12.5^{th} percentiles, respectively, when determining hyper- to intermediate-intensity abnormalities. The results (Figure 5D–F) suggested that lesion quantification by VNE thresholding at the 35th percentile, for example, are directly comparable with LGE using the FWHM method (i.e., 50th percentile), making this version of VNE highly promising to replace LGE in HCM lesion assessment. On the full test set, LGE and threshold-adjusted VNE reported similar average values of hyper- to intermediate-intensity lesions (LGE: 9.8%, 26.1%, 44.4%, versus VNE: 9.9%, 24.1%, 43.9%; Table I in the Supplement). VNE with

adjusted thresholds also highlights the signals of subtle abnormalities for easier visualization (Figure 5E and F, arrowed). There were no false-positive VNE cases, where good quality VNE had introduced lesions in patients with good quality negative LGE by the conventional contrast-enhanced method.

Discussion

In this work, an AI technology was presented that translates native T1-maps (together with cines) into the widely-recognized presentation of LGE, a format immediately ready for standard clinical interpretation. The AI deep learning is effectively acting as a "virtual contrast agent" that enhances the native CMR. In other words, it produces a "virtual LGE" image without the need for gadolinium. This work showed that: (1) virtual native enhancement (VNE) images had significantly better quality than LGE images; and (2) lesion burden quantification by VNE correlated well with LGE, both on a visuospatial (Figure 4) and quantitative (Figure 5) basis. The VNE technology has the potential to change the current paradigm for CMR imaging, as it may allow significantly faster, lower-cost and contrast-free CMR scans, enabling frequent monitoring of myocardial tissue changes.

Advantages of VNE over LGE

Conventional LGE is dependent on intravenous administration of GBCA, and requires at least 10 minutes post GBCA to develop the contrast redistribution [31]. LGE image quality is dependent on appropriate adjustment of TI, although the PSIR technique is less sensitive to TI setting. In comparison, VNE requires no intravenous access or GBCA, is derived from native imaging, and can be repeated as required to confirm findings and ensure sufficient image quality, without concerns about contrast agent wash-out. VNE employs readily-available conventional cine and T1-mapping sequences, which can be completed within 15 minutes, limiting the likelihood of image artefacts due to patient fatigue. VNE showed significantly greater image quality and more consistent image contrast than LGE (Figure 3).

Lesion assessment by VNE and LGE

VNE showed strong agreement with LGE in myocardial lesion visuospatial distribution and quantification. The ICC of 0.77 to 0.87 and a 95% CI of ~20% for inter-method comparison appears to be excellent in view of the reported LGE intra-method variability of ICC at 0.88 [29] and inter-laboratory inconsistencies of 10–15% [32]. Above the linear correlation trend, there is a perceivable skew of enhanced signals in VNE (Figure 5, arrowed). While much work remains to confirm the clinical utility of detecting subtle lesions (often also seen in LGE), this sensitivity appears to arise directly from features of native T1-mapping, in line with literature reporting sensitivity of T1 to early myocardial changes in HCM patients [14, 15, 33].

Deep learning contrast enhancement mechanism

The concept of deep learning contrast enhancement emerged very recently with the advancement in AI methods. In CMR, although the term "synthetic" LGE (generated by deep learning) exists [34–36], they were designed for multi-modal image registration and not

to generate lesion signals. In brain MRI, "virtual gadolinium enhancement" [37, 38] aimed to reduce the contrast dose while predicting the full-dose image signals, but with notable degradation in quality and sensitivity, and with no application to image the heart.

CMR is inherently multi-modal, with each modality demonstrating unique sensitivities to certain pathophysiologies. Previous T1-mapping development suggested that pursuing exact reproduction of conventional modalities (such as LGE) may hinder the potential of the new technology to detect pathologies over standard methods [39, 40]. Therefore, VNE focused on enhancing existing native CMR signals. As a result, in addition to good agreement with LGE, the VNE technology also better displays the subtle lesions often seen in HCM patients.

Limitations and future work

The current VNE is trained on LGE PSIR images typically obtained >10 minutes post GBCA administration [11]. Separate training is required to predict other LGE pulse sequences and post-contrast images, for example, early gadolinium enhancement, first pass perfusion and extra-cellular volume fraction mapping. In collaboration with MR vendors, we plan to implement VNE as an inline sequence on the scanner to allow immediate VNE generation after cine and T1-map acquisitions. It can also be implemented for rapid offline analysis by third-party software vendors.

Individual imaging features may distinguish LGE from VNE and introduce observer bias in image quality assessment; reassuringly, there were no differences between operators who were aware of the study design (MKB, MS) and those who were not (CN, RM). The VNE-LGE agreement appeared to be higher with better image quality (Figure V in the Supplement); future work is needed to test the association between image quality and diagnostic accuracy. The mechanism(s) of how each pre-contrast component contributes to the VNE signals is to be investigated using deep learning visualization techniques [41, 42].

Before recommendation for wide clinical use of VNE, further work is planned to link VNE-detected signals to patient outcomes. VNE may be expanded in future by adding more native modalities, such as T2-mapping or MR fingerprinting [43]. VNE variants developed on different cardiac disease datasets and native modalities can potentially differentiate between pathophysiologic changes, such as oedema, fibrosis and microvascular obstruction.

Clinical impact

T1-mapping interpretation.—Clinical translation of T1-mapping is hindered by non-standardized image interpretation methods [44]. VNE has now addressed this challenge by translating T1-maps into the common language of LGE, whose interpretation is widely accepted and understood in routine clinical practice. Further, it provides a deep learning framework to enhance T1-maps with additional native CMR modalities, demonstrated in this work with pre-contrast cines.

HCM assessment.—The proposed VNE technology is of potentially high clinical impact to HCM patients, who often undergo serial CMRs to monitor disease progression. VNE can obviate repeated administration of GBCA and allow more frequent CMR follow-ups.

Subject to further validation by the planned HCMR study outcomes, the apparent VNE signals to subtle lesions (inherited from T1-mapping) may potentially lead to better HCM risk stratification and treatment, especially given new, potentially disease-modifying therapies for HCM on the horizon [45–48].

GBCA-free CMR.—By expanding the training material to a wider range of pathologies, It is envisaged that VNE could lead to a novel, GBCA-free CMR scanning protocol for myocardial tissue characterization, compatible with the standard clinical interpretation like for GBCA-based LGE. This could expand the capabilities of CMR to include patients in whom GBCAs are contraindicated, ultimately leading to increased patient benefit, satisfaction, and clinical throughput.

Cost-savings.—Currently, the majority of CMR scans for tissue characterization requires intravenous access, the use of GBCA, related consumables and patient preparation by trained staff. VNE is available immediately after native T1-mapping acquisition with no additional cost. Replacing LGE with VNE can significantly shorten the scan time to within 15 minutes, allowing twice as many patients to benefit from CMR at the same infrastructure capacity. The clinical impact and potential cost savings of popularizing this new CMR technology could be substantial.

Conclusions

Virtual Native Enhancement (VNE) imaging is a new CMR technology that resembles conventional LGE, without the need for GBCA administration. VNE achieved a high agreement with LGE in the visuospatial distribution and quantification of lesion burden, with significantly better image quality. While currently validated in the HCM population, there is a clear pathway to extend the technology to a wider range of myocardial pathologies. VNE has enormous potential to significantly improve clinical practice, reduce scan time and costs, and expand the reach of CMR in the near future.

Supplementary Material

Refer to Web version on PubMed Central for supplementary material.

Acknowledgement

Non-standard Abbreviations and Acronyms:

AI	Artificial Intelligence
CMR	Cardiovascular Magnetic Resonance
FWEM	Full Width at Eighth Maximum
FWHM	Full Width at Half Maximum
FWQM	Full Width at Quarter Maximum
GBCA	Gadolinium-based Contrast Agent
HCM	Hypertrophic Cardiomyopathy
HCMR	Hypertrophic Cardiomyopathy Registry
ICC	Intraclass Correlation Coefficients
IRW	Inversion Recovery-Weighted
LGE	Late Gadolinium Enhancement
PSIR	Phase-Sensitive Inversion-Recovery
ROI	Region of Interest
TI	Inversion Time
VNE	Virtual Native Enhancement

References

1. Kim RJ, Wu E, Rafael A, Chen E-L, Parker MA, Simonetti O, Klocke FJ, Bonow RO, and Judd R.M.J.N.E.J.o.M., The use of contrast-enhanced magnetic resonance imaging to identify reversible myocardial dysfunction. 2000; 343: 1445–1453.

2. Bruder O, Wagner A, Lombardi M, Schwitter J, van Rossum A, Pilz G, Nothnagel D, Steen H, Petersen S, Nagel E, et al., European cardiovascular magnetic resonance (EuroCMR) registry – multi national results from 57 centers in 15 countries. Journal of Cardiovascular Magnetic Resonance. 2013; 15: 9. [PubMed: 23331632]

3. Mahrholdt H, Wagner A, Judd RM, Sechtem U, and Kim RJ, Delayed enhancement cardiovascular magnetic resonance assessment of non-ischaemic cardiomyopathies. Eur Heart J. 2005; 26: 1461–74. [PubMed: 15831557]

4. Becker MAJ, Cornel JH, van de Ven PM, van Rossum AC, Allaart CP, and Germans T, The Prognostic Value of Late Gadolinium-Enhanced Cardiac Magnetic Resonance Imaging in Nonischemic Dilated Cardiomyopathy: A Review and Meta-Analysis. JACC: Cardiovascular Imaging. 2018; 11: 1274–1284. [PubMed: 29680351]

5. Gerber BL, Rousseau MF, Ahn SA, le Polain de Waroux JB, Pouleur AC, Phlips T, Vancraeynest D, Pasquet A, and Vanoverschelde JL, Prognostic value of myocardial viability by delayed-enhanced magnetic resonance in patients with coronary artery disease and low ejection fraction: impact of revascularization therapy. J Am Coll Cardiol. 2012; 59: 825–35. [PubMed: 22361403]

6. Gersh BJ, Maron BJ, Bonow RO, Dearani JA, Fifer MA, Link MS, Naidu SS, Nishimura RA, Ommen SR, Rakowski H, et al., 2011 ACCF/AHA Guideline for the Diagnosis and Treatment of Hypertrophic Cardiomyopathy. 2011; 124: e783–e831.

7. Burrage MK and Ferreira VM, Cardiovascular Magnetic Resonance for the Differentiation of Left Ventricular Hypertrophy. Current Heart Failure Reports. 2020; 17: 192–204. [PubMed: 32844347]

8. Elliott PM, Anastasakis A, Borger MA, Borggrefe M, Cecchi F, Charron P, Hagege AA, Lafont A, Limongelli G, Mahrholdt H, et al., 2014 ESC Guidelines on diagnosis and management of hypertrophic cardiomyopathy: The Task Force for the Diagnosis and Management of Hypertrophic Cardiomyopathy of the European Society of Cardiology (ESC). European Heart Journal. 2014; 35: 2733–2779. [PubMed: 25173338]

9. Weng Z, Yao J, Chan RH, He J, Yang X, Zhou Y, and He Y, Prognostic Value of LGE-CMR in HCM: A Meta-Analysis. JACC Cardiovasc Imaging. 2016; 9: 1392–1402. [PubMed: 27450876]

10. Ommen SR, Mital S, Burke MA, Day SM, Deswal A, Elliott P, Evanovich LL, Hung J, Joglar JA, Kantor P, et al., 2020 AHA/ACC Guideline for the Diagnosis and Treatment of Patients With Hypertrophic Cardiomyopathy. Circulation. 2020; 142: e558–e631. [PubMed: 33215931]

11. Kramer CM, Appelbaum E, Desai MY, Desvigne-Nickens P, DiMarco JP, Friedrich MG, Geller N, Heckler S, Ho CY, Jerosch-Herold M, et al., Hypertrophic Cardiomyopathy Registry: The rationale and design of an international, observational study of hypertrophic cardiomyopathy. American Heart Journal. 2015; 170: 223–230. [PubMed: 26299218]

12. U.S. Food & Drug Administration. FDA Drug Safety Communication: FDA wanrs that gadolinium-based contrast agents (GBCAs) are retained in the body; requires new class warnings. Updated5/16/2018. Available from: https://www.fda.gov/drugs/drug-safety-and-availability/fda-drug-safety-communication-fda-warns-gadolinium-based-contrast-agents-gbcas-are-retained-body.

13. Messroghli DR, Moon JC, Ferreira VM, Grosse-Wortmann L, He T, Kellman P, Mascherbauer J, Nezafat R, Salerno M, and Schelbert EB, Clinical recommendations for cardiovascular magnetic resonance mapping of T1, T2, T2* and extracellular volume: a consensus statement by the Society for Cardiovascular Magnetic Resonance (SCMR) endorsed by the European Association for Cardiovascular Imaging (EACVI). Journal of Cardiovascular Magnetic Resonance. 2017; 19: 75. [PubMed: 28992817]

14. Xu J, Zhuang B, Sirajuddin A, Li S, Huang J, Yin G, Song L, Jiang Y, Zhao S, and Lu MJR, MRI T1 mapping in hypertrophic cardiomyopathy: evaluation in patients without late gadolinium enhancement and hemodynamic obstruction. Radiology. 2020; 294: 275–286. [PubMed: 31769741]

15. Dass S, Suttie JJ, Piechnik SK, Ferreira VM, Holloway CJ, Banerjee R, Mahmod M, Cochlin L, Karamitsos TD, Robson MD, et al., Myocardial Tissue Characterization Using Magnetic Resonance Noncontrast T1 Mapping in Hypertrophic and Dilated Cardiomyopathy. Circulation: Cardiovascular Imaging. 2012; 5: 726–733. [PubMed: 23071146]

16. Lu M, Zhao S, Yin G, Jiang S, Zhao T, Chen X, Tian L, Zhang Y, Wei Y, and Liu Q.J.E.j.o.r., T1 mapping for detection of left ventricular myocardial fibrosis in hypertrophic cardiomyopathy: a preliminary study. European Journal of Radiology. 2013; 82: e225–e231. [PubMed: 23333530]

17. Bull S, White SK, Piechnik SK, Flett AS, Ferreira VM, Loudon M, Francis JM, Karamitsos TD, Prendergast BD, Robson MD, et al., Human non-contrast T1 values and correlation with histology in diffuse fibrosis. Heart2013; 99: 932–937. [PubMed: 23349348]

18. Bing R and Dweck MR, Myocardial fibrosis: why image, how to image and clinical implications. Heart. 2019; 105: 1832–1840. [PubMed: 31649047]

19. Diao K. y., Yang Z.-g., Xu H.-y., Liu X, Zhang Q, Shi K, Jiang L, Xie L.-j., Wen L.-y., and Guo Y.-k., Histologic validation of myocardial fibrosis measured by T1 mapping: a systematic review and meta-analysis. Journal of Cardiovascular Magnetic Resonance. 2016; 18: 92. [PubMed: 27955698]

20. Schelbert EB and Messroghli DR, State of the art: clinical applications of cardiac T1 mapping. Radiology. 2016; 278: 658–676. [PubMed: 26885733]

21. Ronneberger O, Fischer P, and Brox T. U-net: Convolutional networks for biomedical image segmentation. in International Conference on Medical image computing and computer-assisted intervention. 2015. Springer: 234–241.

22. Isola P, Zhu J-Y, Zhou T, and Efros AA. Image-to-image translation with conditional adversarial networks. in Proceedings of the IEEE conference on computer vision and pattern recognition. 2017. 1125–1134.

23. Simonyan K and Zisserman A, Very deep convolutional networks for large-scale image recognition. arXiv. preprint posted April 10, 2015. doi: arXiv:1409.1556.

24. Piechnik SK, Ferreira VM, Dall'Armellina E, Cochlin LE, Greiser A, Neubauer S, and Robson MD, Shortened Modified Look-Locker Inversion recovery (ShMOLLI) for clinical myocardial T1-mapping at 1.5 and 3 T within a 9 heartbeat breathhold. Journal of Cardiovascular Magnetic Resonance. 2010; 12: 69. [PubMed: 21092095]

25. Zhang Q, Werys K, Popescu IA, Biasiolli L, Ntusi NAB, Desai M, Zimmerman SL, Shah DJ, Autry K, Kim B, et al., Quality assurance of quantitative cardiac T1-mapping in multicenter clinical trials – A T1 phantom program from the hypertrophic cardiomyopathy registry (HCMR) study. International Journal of Cardiology. 2021; 330: 251–258. [PubMed: 33535074]

26. Kellman P, Arai AE, McVeigh ER, and Aletras AH, Phase-sensitive inversion recovery for detecting myocardial infarction using gadolinium-delayed hyperenhancement. Magnetic Resonance in Medicine. 2002; 47: 372–383. [PubMed: 11810682]

27. Hann Evan, Popescu Iulia, Zhang Qiang, Gonzales Ricardo, Barutcu Ahmet, Neubauer Stefan, Ferreira Vanessa M., and Piechnik SK, Deep Neural Network Ensemble for On-the-Fly Quality Control-Driven Segmentation of Cardiac MRI T1 Mapping. Medical Image Analysis. 2021; 71: 102029. [PubMed: 33831594]

28. Gräni C, Eichhorn C, Bière L, Kaneko K, Murthy VL, Agarwal V, Aghayev A, Steigner M, Blankstein R, Jerosch-Herold M, et al., Comparison of myocardial fibrosis quantification methods by cardiovascular magnetic resonance imaging for risk stratification of patients with suspected myocarditis. Journal of Cardiovascular Magnetic Resonance. 2019; 21: 14. [PubMed: 30813942]

29. Mikami Y, Kolman L, Joncas SX, Stirrat J, Scholl D, Rajchl M, Lydell CP, Weeks SG, Howarth AG, and White JA, Accuracy and reproducibility of semi-automated late gadolinium enhancement quantification techniques in patients with hypertrophic cardiomyopathy. Journal of Cardiovascular Magnetic Resonance. 2014; 16: 85. [PubMed: 25315701]

30. Appelbaum E, Maron BJ, Adabag S, Hauser TH, Lesser JR, Haas TS, Riley AB, Harrigan CJ, Delling FN, Udelson JE, et al., Intermediate-Signal-Intensity Late Gadolinium Enhancement Predicts Ventricular Tachyarrhythmias in Patients With Hypertrophic Cardiomyopathy. Circulation: Cardiovascular Imaging. 2012; 5: 78–85. [PubMed: 22135401]

31. Kramer CM, Barkhausen J, Bucciarelli-Ducci C, Flamm SD, Kim RJ, and Nagel E, Standardized cardiovascular magnetic resonance imaging (CMR) protocols: 2020 update. Journal of Cardiovascular Magnetic Resonance. 2020; 22: 17. [PubMed: 32089132]

32. Klem I, Heiberg E, Van Assche L, Parker MA, Kim HW, Grizzard JD, Arheden H, and Kim RJ, Sources of variability in quantification of cardiovascular magnetic resonance infarct size - reproducibility among three core laboratories. Journal of Cardiovascular Magnetic Resonance. 2017; 19: 62. [PubMed: 28800739]

33. Hashimura H, Kimura F, Ishibashi-Ueda H, Morita Y, Higashi M, Nakano S, Iguchi A, Uotani K, Sugimura K, and Naito H, Radiologic-Pathologic Correlation of Primary and Secondary Cardiomyopathies: MR Imaging and Histopathologic Findings in Hearts from Autopsy and Transplantation. RadioGraphics. 2017; 37: 719–736. [PubMed: 28129067]

34. Zhuang X, Xu J, Luo X, Chen C, Ouyang C, Rueckert D, Campello VM, Lekadir K, Vesal S, and RaviKumar N, Cardiac segmentation on late gadolinium enhancement MRI: a benchmark study from multi-sequence cardiac MR segmentation challenge. arXiv. preprint posted June 22, 2020. doi: arXiv:2006.12434. 2020.

35. Chen C, Ouyang C, Tarroni G, Schlemper J, Qiu H, Bai W, and Rueckert D. Unsupervised Multi-modal Style Transfer for Cardiac MR Segmentation. in International Workshop on Statistical Atlases and Computational Models of the Heart. 2019. Springer: 209–219.

36. Campello VM, Martín-Isla C, Izquierdo C, Petersen SE, Ballester MAG, and Lekadir K. Combining Multi-Sequence and Synthetic Images for Improved Segmentation of Late Gadolinium Enhancement Cardiac MRI. in International Workshop on Statistical Atlases and Computational Models of the Heart. 2019. Springer: 290–299.

37. Gong E, Pauly JM, Wintermark M, and Zaharchuk G, Deep learning enables reduced gadolinium dose for contrast-enhanced brain MRI. Journal of magnetic resonance imaging. 2018; 48: 330–340. [PubMed: 29437269]

38. Kleesiek J, Morshuis JN, Isensee F, Deike-Hofmann K, Paech D, Kickingereder P, Köthe U, Rother C, Forsting M, and Wick W, Can virtual contrast enhancement in brain MRI replace gadolinium?: a feasibility study. Investigative radiology. 2019; 54: 653–660. [PubMed: 31261293]

39. Robson MD, Piechnik SK, Tunnicliffe EM, and Neubauer S, T1 measurements in the human myocardium: The effects of magnetization transfer on the SASHA and MOLLI sequences. Magnetic Resonance in Medicine. 2013; 70: 664–670. [PubMed: 23857710]

40. Piechnik SK, Neubauer S, and Ferreira VM, State-of-the-art review: stress T1 mapping-technical considerations, pitfalls and emerging clinical applications. Magma. 2018; 31: 131–141. [PubMed: 28914389]

41. Jetley S, Lord NA, Lee N, and Torr PH, Learn to pay attention. arXiv. preprint posted April 26, 2018. doi: arXiv:1804.02391.

42. Zhang Q, Hann E, Werys K, Wu C, Popescu I, Lukaschuk E, Barutcu A, Ferreira VM, and Piechnik S.K.J.A.i.i.m., Deep learning with attention supervision for automated motion artefact detection in quality control of cardiac T1-mapping. 2020; 110: 101955.

43. Ma D, Gulani V, Seiberlich N, Liu K, Sunshine JL, Duerk JL, and Griswold MA, Magnetic resonance fingerprinting. Nature. 2013; 495: 187–192. [PubMed: 23486058]

44. Popescu IA, Werys K, Zhang Q, Puchta H, Hann E, Lukaschuk E, Ferreira VM, and Piechnik SK, Standardization of T1-mapping in cardiovascular magnetic resonance using clustered structuring for benchmarking normal ranges. International Journal of Cardiology. 2020; 326: 220–225. [PubMed: 33096146]

45. Repetti GG, Toepfer CN, Seidman JG, and Seidman CE, Novel Therapies for Prevention and Early Treatment of Cardiomyopathies. Circulation research. 2019; 124: 1536–1550. [PubMed: 31120825]

46. Heitner SB, Jacoby D, Lester SJ, Owens A, Wang A, Zhang D, Lambing J, Lee J, Semigran M, and Sehnert A.J.J.A.o.i.m., Mavacamten treatment for obstructive hypertrophic cardiomyopathy: a clinical trial. Annals of internal medicine. 2019; 170: 741–748. [PubMed: 31035291]

47. Saberi S, Cardim N, Yamani MH, Schulz-Menger J, Li W, Florea V, Sehnert AJ, Kwong RY, Jerosch-Herold M, Masri A, et al., Mavacamten Favorably Impacts Cardiac Structure in Obstructive Hypertrophic Cardiomyopathy: EXPLORER-HCM CMR Substudy Analysis. Circulation. 2021; 143: 606–608. [PubMed: 33190524]

48. Robertson LA, Armas DR, Robbie E, Osmukhina A, Li H, Malik FI, and Solomon S.D.J.J.o.C.F., A First in Human Study of the Selective Cardiac Myosin Inhibitor, CK-3773274. Journal of Cardiac Failure. 2019; 25: S79–S80.

49. Johnson J, Alahi A, and Fei-Fei L. Perceptual losses for real-time style transfer and super-resolution. in European conference on computer vision. 2016. Springer: 694–711.

50. Russakovsky O, Deng J, Su H, Krause J, Satheesh S, Ma S, Huang Z, Karpathy A, Khosla A, and Bernstein M, Imagenet large scale visual recognition challenge. International journal of computer vision. 2015; 115: 211–252.

51. Kingma DP and Ba J, Adam: A method for stochastic optimization. arXiv. preprint posted Jan 30, 2017. doi: arXiv:1412.6980.

52. Abadi M, Agarwal A, Barham P, Brevdo E, Chen Z, Citro C, Corrado GS, Davis A, Dean J, and Devin M, Tensorflow: Large-scale machine learning on heterogeneous distributed systems. arXiv. preprint posted March 16, 2016. doi: arXiv:1603.04467.

Clinical Perspective

What is new?

- Virtual Native Enhancement (VNE) is a new deep learning-driven CMR technology that generates images closely resembling conventional LGE without the need for gadolinium-based contrast agent (GBCA); in other words, it serves as a "virtual contrast agent" and produces "virtual LGE" images.

- VNE images achieve high agreement with LGE in the visuospatial distribution and quantification of lesions, with significantly better image quality than LGE.

- VNE offers a new CMR tissue characterization technology that can significantly reduce scan time and obviate the need for contrast agent.

What are the clinical implications?

- For hypertrophic cardiomyopathy (HCM) patients, VNE can obviate repeated administration of GBCA in serial CMR scans for monitoring disease progression.

- While currently validated in HCM, there is a clear pathway to extend VNE to characterize a wider range of cardiac pathologies.

- The VNE technology has the potential to change the current paradigm for CMR imaging, as it may allow significantly faster, lower-cost and contrast-free CMR scans, enabling frequent monitoring of myocardial tissue changes.
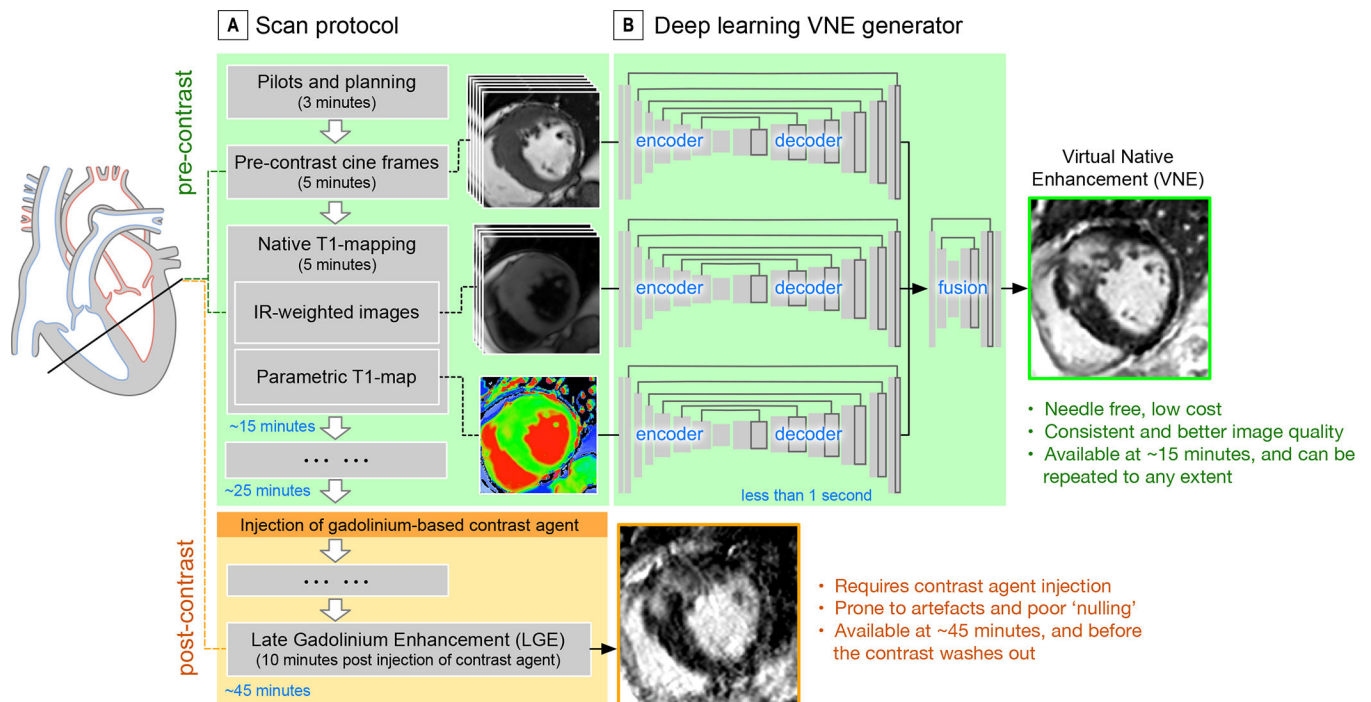
Figure 1. Overview of the Virtual Native Enhancement (VNE) imaging technology.
(A) Simplified illustration of HCMR scan protocol which includes native (pre-contrast) cine, T1-mapping (including native inversion recovery-weighted images), and conventional post-contrast late gadolinium enhancement (LGE). (B) VNE generator. Native CMR images are input to three steams of encoder-decoder U-Nets to extract feature maps, followed by a further neural network block to fuse all feature maps and derive a VNE image. Once trained, producing a VNE image takes less than one second.
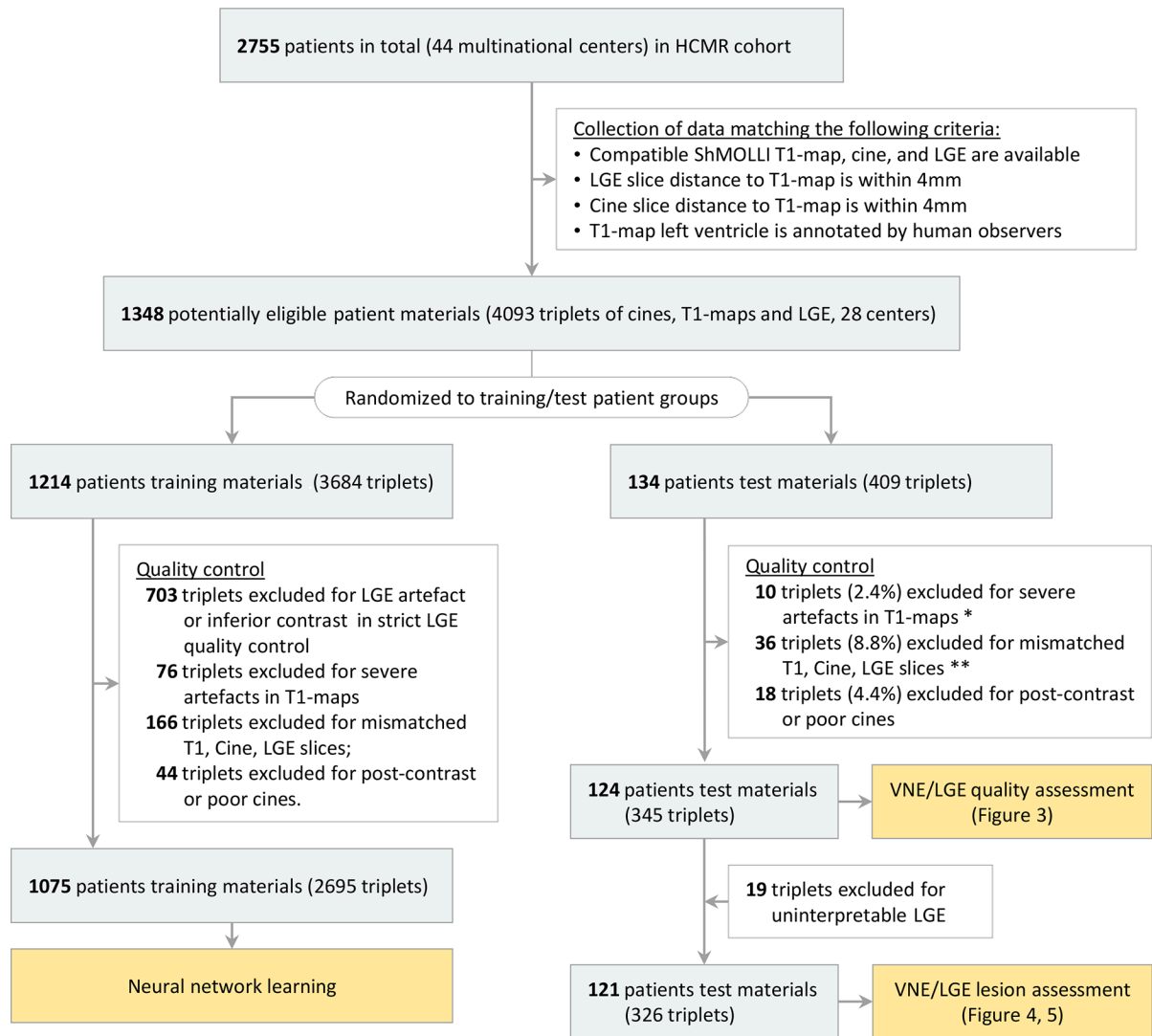
Figure 2. Flow of patient material selection for developing and testing the VNE technology.
*The excluded T1-maps (n=10) in testing materials are disclosed in Figure III in the Supplement. **Four of the 36 triplets were retrospectively excluded from analysis due to slice position mismatch and coil problems identified by consensus of two CMR experts; see Figure IV in the Supplement. These examples were not detected automatically using the pre-defined criteria in slice position matching, and were excluded after manual inspection.
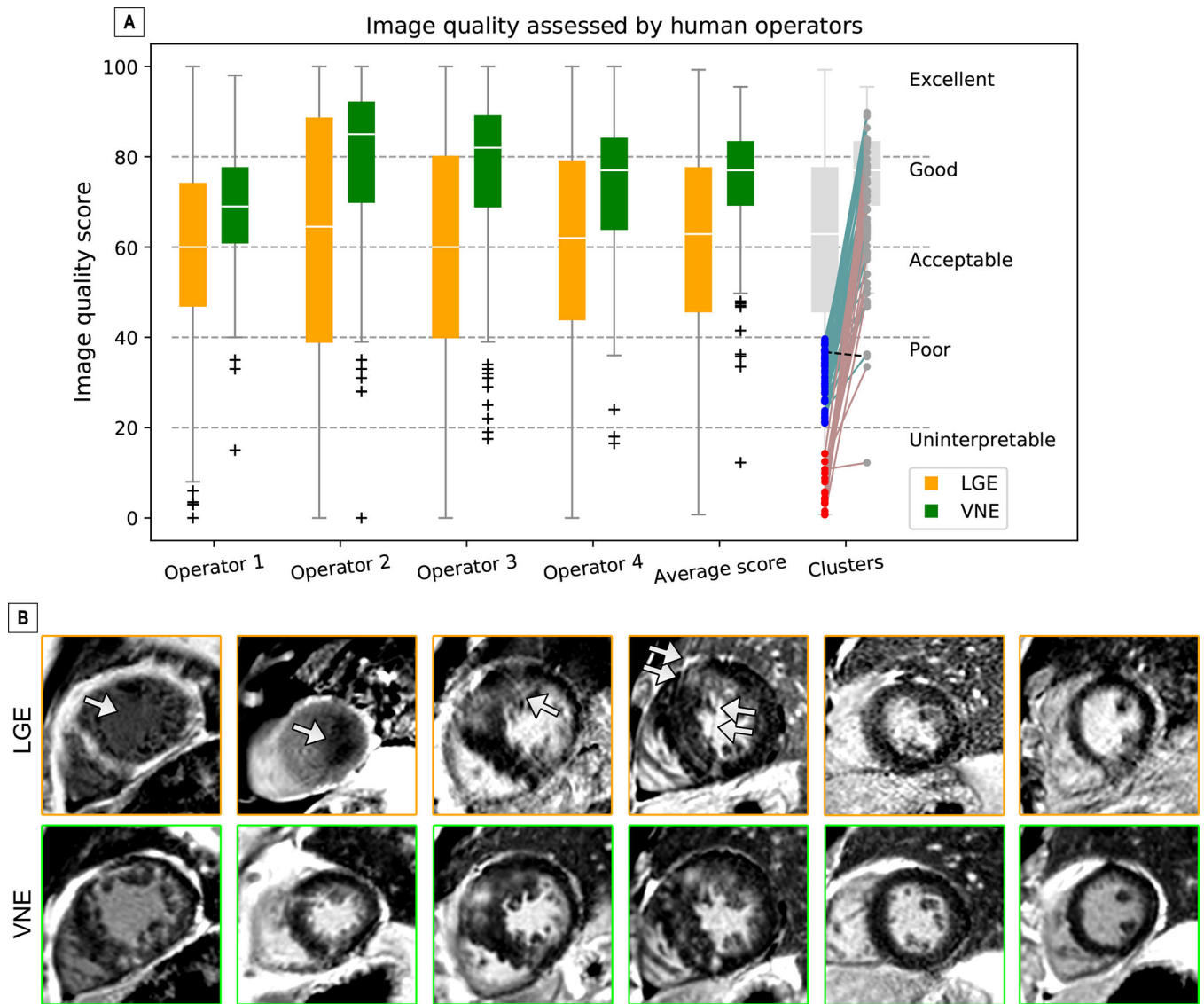
Figure 3. VNE and LGE image quality assessment on 346 test materials (124 patients).
(A) VNE provides significantly better image quality, assessed by four blinded operators and their average scores (all p<0.001). For cases with "uninterpretable" (red clusters) or "poor" (blue) LGE images, VNE provides superior imaging quality in all but one case (dashed line). (B) examples of image quality improvement by VNE, which has more consistent appearance and defined borders. Arrows point to the LGE artefacts.
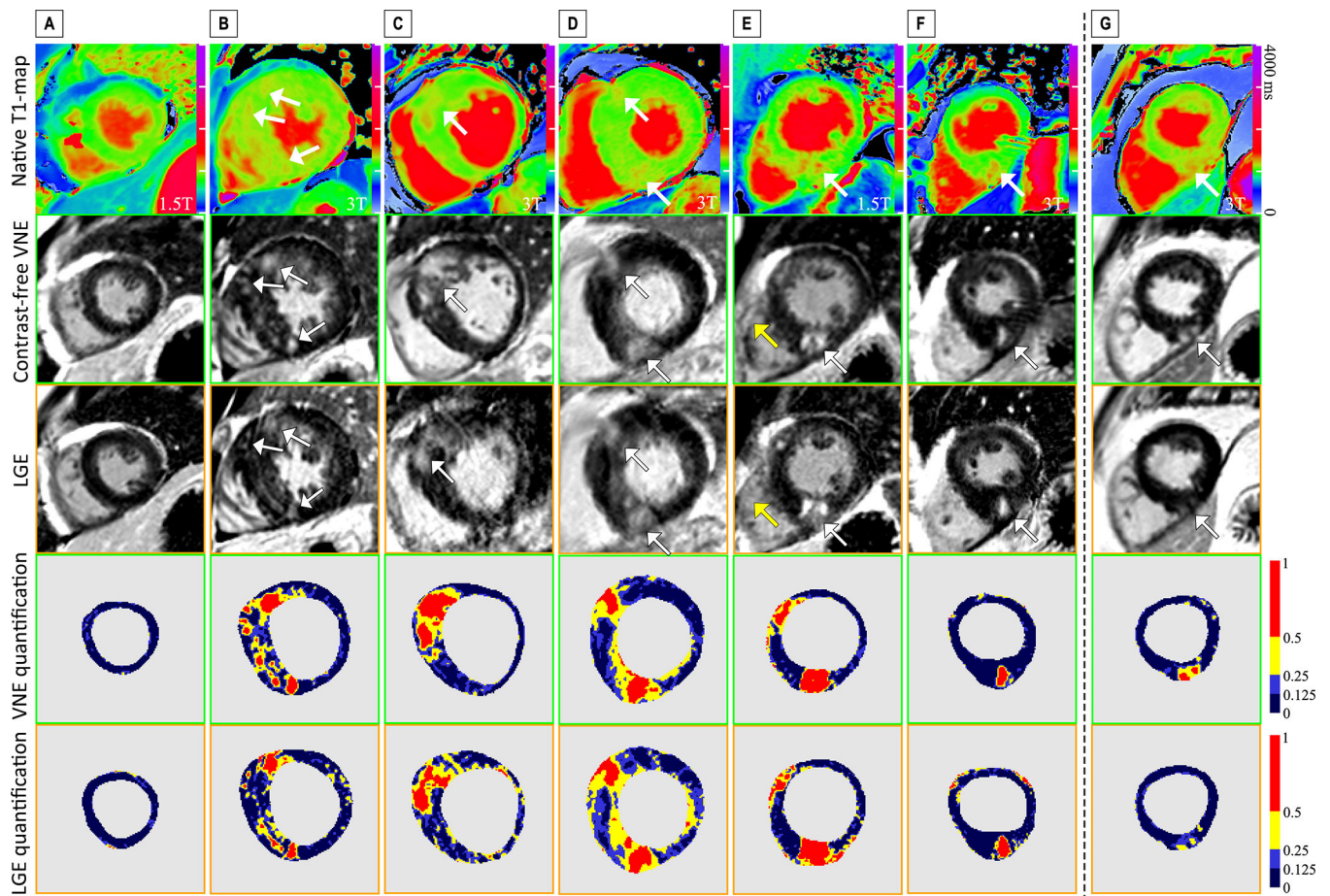
Figure 4. Examples to illustrate visuospatial agreement between VNE and conventional LGE.
T1 colormaps (top row) were adjusted individually to highlight the T1 signals corresponding
to VNE signals. Bottom two rows visualize lesion regions by VNE and LGE using
progressive thresholding (full width at half, a quarter, and eighth maximum, i.e., at 50th,
25th, 12.5th percentiles) displayed with different colors. (A-F) High visuospatial agreement
was observed between VNE and LGE. Yellow arrows point to slightly different right
ventricle sizes in VNE and LGE, suggesting patient movement between acquisitions. (G)
An example of VNE displaying subtle changes clearer than LGE.
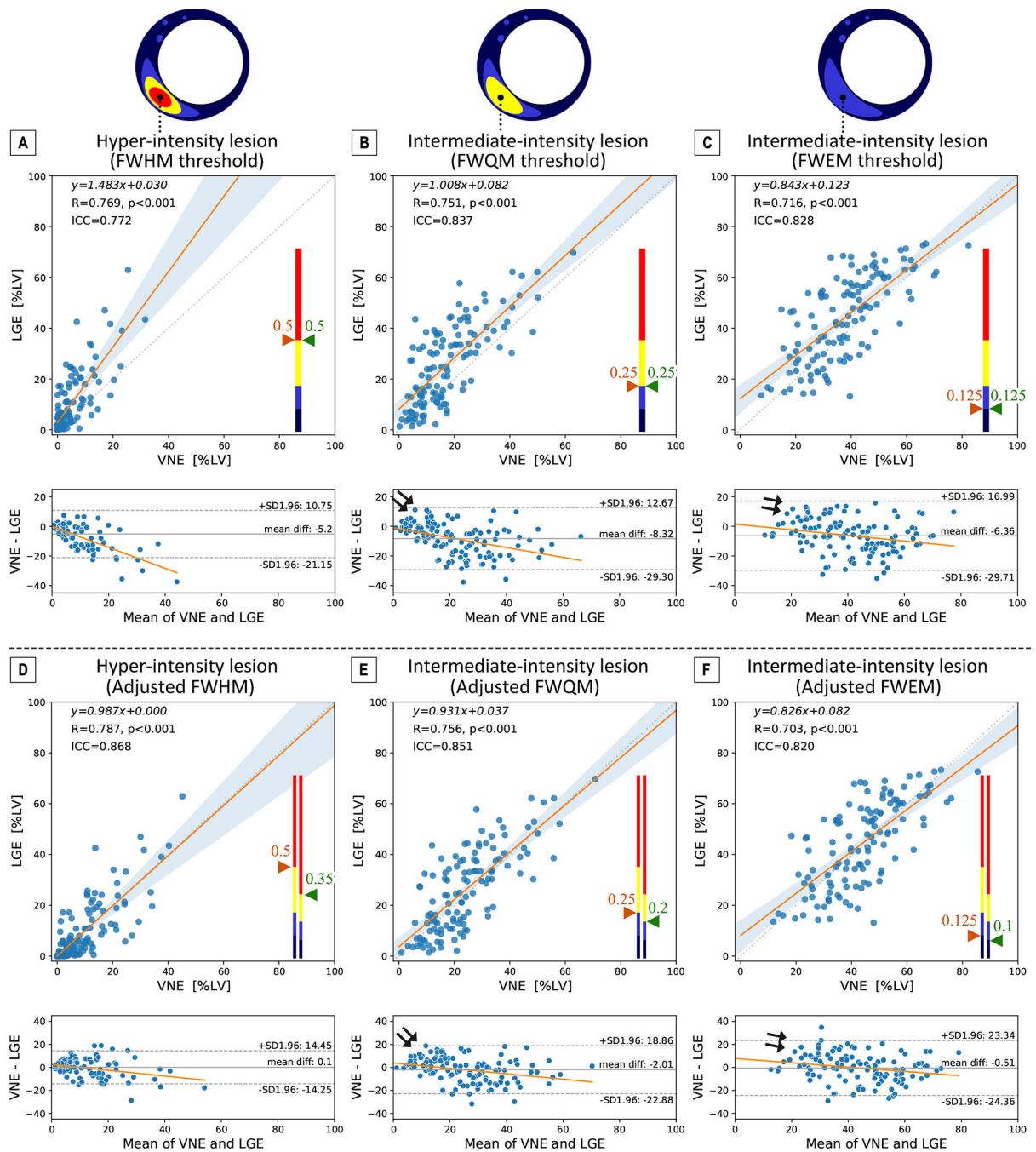
Figure 5. VNE correlated strongly with conventional LGE in quantifying hyper-intensity to intermediate-intensity lesions (left to right) in 121 test patients.

(A-C) use same thresholding methods FWHM, FWQM, FWEM (i.e. thresholding at 50th, 25th, 12.5th percentiles, reflecting hyper-intensity to intermediate-intensity subtle lesions) for VNE and LGE. (D-F) use adjusted thresholding at 35th, 20th, 10th percentiles for VNE. Threshold values are illustrated on color bars. Linear regression equations, correlation coefficient R-values, and ICC are provided. Bland-Altman plots below each

panel demonstrate perceivable trends (arrowed) with associated clustering, suggesting enhanced signals in VNE for subtle lesions.